Postprint of: Kulpa-Koterwa A., Ryl J., Górnicka K., Niedziałkowski P., New nanoadsorbent based on magnetic iron oxide containing 1,4,7,10-tetraazacyclododecane in outer chain ($Fe_3O_4$@$SiO_2$-cyclen) for adsorption and removal of selected heavy metal ions $Cd^{2+}$, $Pb^{2+}$, $Cu^{2+}$, Journal of Molecular Liquids, Vol. 368, Part B (2022), 120710, DOI: 10.1016/j.molliq.2022.120710


# New nanoadsorbent based on magnetic iron oxide containing 1,4,7,10-tetraazacyclododecane in outer chain ($Fe_3O_4$@$SiO_2$-cyclen) for adsorption and removal of selected heavy metal ions $Cd^{2+}$, $Pb^{2+}$, $Cu^{2+}$

**Amanda Kulpa-Koterwa[a], Jacek Ryl[b], Karolina Górnicka[c], Paweł Niedziałkowski[a,*]**

[a] Department of Analytical Chemistry, Faculty of Chemistry, University of Gdansk, Wita Stwosza 63, 80-308 Gdańsk, Poland

[b] Division of Electrochemistry and Surface Physical Chemistry, Institute of Nanotechnology and Materials Engineering and Advanced Materials Center, Gdańsk University of Technology, Narutowicza 11/12, 80-233 Gdańsk, Poland

[c] Faculty of Applied Physics and Mathematics, Advanced Materials Center, Gdansk University of Technology, Narutowicza 11/12, 80-233 Gdansk, Poland

*corresponding author: Paweł Niedziałkowski

e-mail address: pawel.niedzialkowski@ug.edu.pl

## Abstract

Magnetic $Fe_3O_4$@$SiO_2$-cyclen nanoparticles were prepared and used as adsorbent for $Cd^{2+}$, $Pb^{2+}$ and $Cu^{2+}$ from aqueous solution removal process controlled with differential pulse anodic stripping voltammetry (DPASV) and hanging mercury drop electrode (HDME). Nanomaterial was synthesised in three-step process co-precipitation of $Fe_3O_4$ core, coating with silane and N-(3-(triethoxysilyl)propyl)-1,4,7,10-tetraazacyclododecane-1-carboxamide silane functionalisation. The effectiveness of each step of the synthesis was confirmed using scanning electron microscopy (SEM), high-resolution X-ray photoelectron spectroscopy (XPS), powder X-ray diffraction (pXRD) and fourier-transform infrared spectroscopy (FT-IR) techniques. The $Fe_3O_4$@$SiO_2$-cyclen nanoparticles were employed for $Cd^{2+}$, $Pb^{2+}$ and $Cu^{2+}$ ions elimination from individual and mixed solutions by carrying out titration with a suspension of nanocomposites. The binding level for all ions both in the individual solutions and in the mixture was very similar at high levels. For $Cd^{2+}$ and $Cu^{2+}$ ions sorption efficiency level was from 83% to 89%, while for $Pb^{2+}$ ions it was slightly lower at the level over 73%. In all cases, the equilibrium adsorption capacity parameter was over 1 mg/g and reached definitely higher values for individual ions solutions. The research results revealed that $Fe_3O_4$@$SiO_2$- cyclen nanoparticles can be a promising adsorbent for magnetic heavy metal ions water treatment agents.

**Keywords:** functionalised $Fe_3O_4$ nanoparticles, stripping voltammetry, $Cd^{2+}$, $Pb^{2+}$ and $Cu^{2+}$ ions binding, nanoadsorbent, 1,4,7,10-tetraazacyclododecane, heavy metal ions removal

## Highlights

- $Fe_3O_4$@$SiO_2$- cyclen nanoparticles was utilised for the removal of $Cd^{2+}$, $Pb^{2+}$, $Cu^{2+}$.
- The SEM, XPS, pXRD and FT-IR characterisation of nanoparticles was performed.
- Ions binding kinetics and efficiency were investigated with DPASV and HDME.
- Sorption efficiency was calculated and reached a maximum level of nearly 90%.
- The effectiveness of ions magnetic separation from the aqueous solution was confirmed.

## 1. Introduction

Over the last few decades, a significant increase has been observed in environmental pollution with heavy metal ions, which is a problem all over the world [1]. The increasing heavy metal ions concentration is generated mainly by technological and operational activities, production processes such as refining, power plants and combined heat and power plants, steel mills, coal and waste combustion, the chemical industry, the use of fertilisers and pesticides, and transport [2]. The presence of heavy metal ions in the environment constitutes a threat due to the possibility of their migration along the rungs of the trophic chain from soil, air, surface waters to plants, animals and in consequence to humans. Exposure to continuously increasing heavy metal ions concentrations lowers the action of biological barriers, which has a negative impact on human health due to their low biodegradability, bioaccumulation tendency, potential carcinogenic effect and mutagenicity [3]. Due to the danger posed by heavy metal ions environment contamination, the recycling of them from aquatic environments has become a very important area of scientific research and industry.

Until now, many methods of metal ions remediation from the environment have been used [4,5], particularly methods such as membrane filtration [6], osmosis [7], ion exchange [8], extraction with ionic liquids [9], photocatalysts [10], clays/layered double hydroxides [11], bioremediation [12], biomass and biosorption [13] phytoremediation [14], precipitation and coagulation [15,16] or electrocoagulation [17]. The conventional wastewater treatment technologies involving physical, chemical, and biological methods have their advantages but also disadvantages such as high costs, complex working operation, secondary pollutants production, low selectivity and many others [18]. To overcome these challenges, researchers used adsorption process as an alternative due to its wide working potentials, low price, simplicity in use, process efficiency, selectivity, capacity for material regeneration and pollutants trace concentration removal [19,20]. A wide range of materials have found application as heavy metal ions adsorbents e.g., chitosan and its functionalised forms [21], aerogels and their derivatives [22], based on cellulose [23], metal organic frameworks [24], carbon-based materials [25], polymers [26], dendrimers [27] and many others [28–31]. However, among many research groups, various nanoscale adsorbents became very popular due to their high surface area, high mobility in solution, reactivity, good adsorption capacity and in consequence efficiency [32]. A series of nanoparticles and their modification were investigated as heavy metal adsorbents but, in recent years, a particular interest was attached to nanoparticles with magnetic properties, especially magnetite $Fe_3O_4$ [33,34]. Magnetite

nanoparticles occupy a special importance due to the possibility of easy and quick isolation with the use of an external magnetic field [35]. Furthermore, creating core-shell type structures with silica $Fe_3O_4$@$SiO_2$ provides a good basis for further functionalisation thus for obtaining a material with wide applicability and selectivity [36–38]. There are known plenty of $Fe_3O_4$@$SiO_2$ modified structures for heavy metal ions adsorption, however, the search for new and selective composites is still topical [39–41]. So far, there is lack of knowledge about crown ethers usage as surface nanocomposites modifiers. Qin et al. designed and synthesised silica gel bound di(aminobenzo)-18-crown-6(SGN18) for zirconium and hafnium adsorption [42]. Aza-crown ethers and derivatives in their heyday were widely used as complexation agents of metal ions in wide range of applications [43,44]. One of the well-known and widely used agent as a metal ions complexation was 1,4,7,10-tetraazacyclododecane [45–49].

In view of the fact that previously the authors used $Fe_3O_4$@$SiO_2$ nanoparticles containing nitrogen atoms in the outer chain as heavy metal ion adsorbent [50,51], they now decided to combine the excellent complexing properties of 1,4,7,10-tetraazacyclododecane and the possibility of pollutants magnetic isolation. In this work, magnetic core-shell nanoparticles functionalised with 1,4,7,10-tetraazacyclododecane $Fe_3O_4$@$SiO_2$-cyclen were designed, synthesised and used as heavy metal $Cd^{2+}$, $Pb^{2+}$, and $Cd^{2+}$ ions adsorbent for the first time. The newly obtained nanomaterial was characterised at every stage of synthesis using SEM, FT-IR, pXRD and (XPS) methods. Furthermore, the ions binding kinetics studies was performed and the binding capacity of nanoparticles was investigated using the differential pulse anodic stripping voltammetry (DPASV) method coupled with hanging mercury drop electrode (HDM) electrode. It is worth mentioning that the application of electrochemical detection skips conventional techniques' limitations in heavy metal detection and offers the same sensitivity with a lower cost, less complex operational procedures and fast on-site detection [52].

## 2. Experimental

### 2.1. Reagents

All analytical grade reagents were purchased from the indicated suppliers and used without further purification. All inorganic salts – ferric chloride hexahydrate ($FeCl_3 \cdot 6H_2O$), ferrous chloride tetrahydrate ($FeCl_2 \cdot 4H_2O$), potassium chloride KCl (99.9%), cadmium nitrate tetrahydrate $Cd(NO_3)_2 \cdot 4H_2O$ (99.9%), lead nitrate $Pb(NO_3)_2$, and copper nitrate trihydrate $Cu(NO_3)_2 \cdot 3H_2O$ (99.9%) – were purchased from POCh (Poland). The organic solvents, ammonia (25%), tetraethylorthosilicate (98%) (TEOS), triethoxy(3-isocyanatopropyl)silane

were purchased from Sigma-Aldrich (Poland). 1,4,7,10-tetraazacyclododecane was bought from Strem Chemicals. Aqueous solutions were prepared using ultra-pure deionised water.

### 2.2. Synthesis of core-shell $Fe_3O_4$@$SiO_2$-cyclen nanostructures

New functionalised nanocomposites were obtained in the three-steps synthesis process. In the first stage, a magnetic $Fe_3O_4$ core was received by the co-precipitation method. The mixture of $Fe^{2+}$($FeCl_2 \cdot 4H_2O$) and $Fe^{3+}$ ($FeCl_3 \cdot 6H_2O$) in aqueous solution using a three-neck flask was stirred under nitrogen conditions. Then the 25% ammonia solution was dripped into the reaction until the pH reached 11. Then the reaction mixture was heated to 60 °C for 3 hours to complete precipitation of the magnetite. The obtained nanoparticles were separated by a magnet and washed with distilled water several times.

The second stage of the synthesis involved the nanomagnetite coating with silica forming $Fe_3O_4$@$SiO_2$, which was used for further modification. 16 g of $Fe_3O_4$ nanoparticles obtained in the previous stage was dispersed in a mixture of 240 mL EtOH and 60 ml $H_2O$. Then 3 mL of TEOS was added into reaction and the reaction was heated overnight to 50 °C. After this time, the obtained nanoparticles were magnetically collected and washed with distilled water several times.

In next stage of synthesis it was necessary to synthesise a modifier of the obtained nanoparticles $Fe_3O_4$@$SiO_2$ due to the fact that the silane derivatives containing 1,4,7,10-tetraazacyclododecane are not a commercially available.

The reaction of 1,4,7,10-tetraazacyclododecane with triethoxy(3-isocyanatopropyl)silane was performed according to the modified procedure described previously [53] to obtain N-(3-(triethoxysilyl)propyl)-1,4,7,10-tetraazacyclododecane-1-carboxamide.

To the solution of 1,4,7,10-tetraazacyclododecane (4.179 g, 24,256 mmol) dissolved in 200 ml dichloromethane 6 mL of triethoxy(3-isocyanatopropyl)silane (24,256 mmol) was dropwise added and the reaction was carried out overnight at 40 °C under a reflux condenser. Then the solvent was evaporated under reduced pressure. The obtained colourless oil was dried in a vacuum desiccator over $P_2O_5$ to obtain 2.159 g of colourless solid with a yield of 21.33%.
MALDI-TOF MS: m/z 419,29 $[M+H]^+$, (MW = 420.31).
IR (KBr) ($cm^{-1}$): 3291, 2972, 2926, 2886, 2735, 1627, 1536, 1478, 1444, 1391, 1365, 1254, 1189, 1165, 1103, 1078, 955, 784.
$^1$H-NMR ($CDCl_3$): 0.538-0.572 (t, 2H, $(CH_3\text{-}CH_2)_3SiO\text{-}\underline{CH_2}\text{-}CH_2\text{-}CH_2\text{-}HN$-, $J_1$ = 7 Hz; $J_1$ = 10,0 Hz; $J_2$=8,5 Hz); 1.135-1.165 (dt, 9H, $(\underline{CH_3}\text{-}CH_2)_3SiO\text{-}CH_2\text{-}CH_2\text{-}CH_2\text{-}HN$-, $J_1$=1 Hz;

$J_1$ = 1,5 Hz; $J_1$ = $J_2$ = 7.0 Hz); 1.479-1.623 (m, 2H, $(CH_3\text{-}CH_2)_3SiO\text{-}CH_2\text{-}\underline{CH_2}\text{-}CH_2\text{-}HN\text{-}$); 2.564-3.652 (m, 18H, $(CH_3\text{-}CH_2)_3SiO\text{-}CH_2\text{-}CH_2\text{-}\underline{CH_2}\text{-}HN\text{- -}H\text{-}\underline{CH_2}\text{-}\underline{CH_2}\text{-}N\text{-,}$); 3.734-3.754 (q, 6H, $(CH_3\text{-}\underline{CH_2})_3SiO\text{-}CH_2\text{-}CH_2\text{-}CH_2\text{-}HN\text{-}$, $J_1$=3 Hz; $J_1$ = 4 Hz; $J_3$ = $J_4$ = 3.0 Hz);

The third stage consisted of $Fe_3O_4$@$SiO_2$ modification to obtain $Fe_3O_4$@$SiO_2$-cyclen. 1.593 g of $Fe_3O_4$@$SiO_2$ was added to a solution of (3.324 g, 7,928 mmol) N-(3-(triethoxysilyl)propyl)-1,4,7,10-tetraazacyclododecane-1-carboxamide dissolved in 150 mL toluene. Then the reaction mixture was stirred for 12 h at 120 ºC. After cooling to room temperature the obtained product was magnetically collected and washed several times with toluene and then with methanol. The resulting product was air-dried.

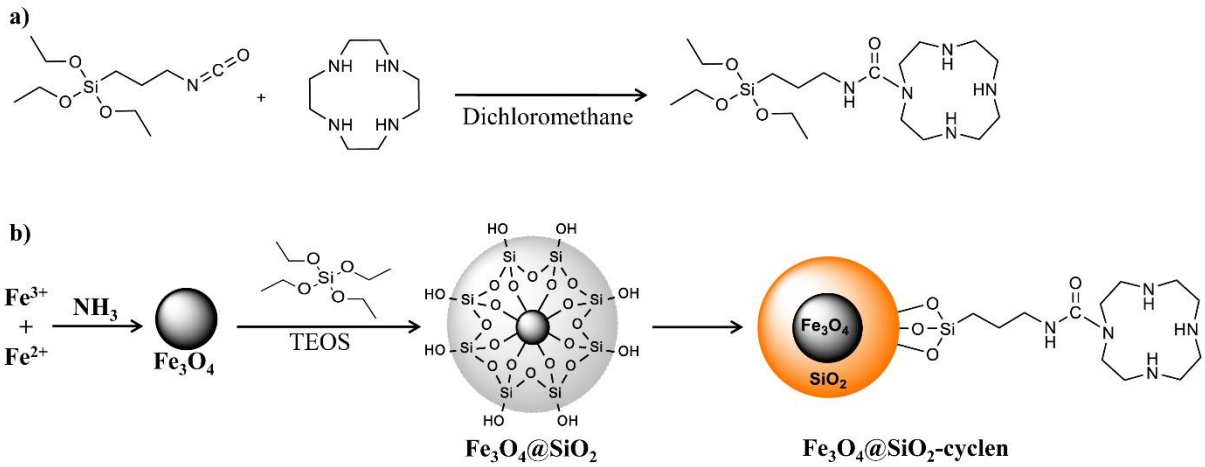


**Figure 1.** Scheme of a) nanoparticles modifier N-(3-(triethoxysilyl)propyl)-1,4,7,10-tetraazacyclododecane-1-carboxamide and b) functionalised $Fe_3O_4$@$SiO_2$-cyclen nanocomposite synthesis.

### 2.3. The $Cd^{2+}$, $Pb^{2+}$ and $Cu^{2+}$ ions removal experiments from aqueous solutions by $Fe_3O_4$@$SiO_2$-cyclen binding

The removal experiments of $Cd^{2+}$, $Pb^{2+}$ and $Cu^{2+}$ ions from aqueous solutions were performed by titration with $Fe_3O_4$@$SiO_2$-cyclen nanoparticles. The ions-binding abilities of $Fe_3O_4$@$SiO_2$-cyclen were studied in the solutions containing both individual ion or the mixture of $Cd^{2+}$, $Pb^{2+}$ and $Cu^{2+}$ ions in concentration level $4.5\cdot10^{-6}$ M. Before starting (DPASV) measurement a 0.25 mg of $Fe_3O_4$@$SiO_2$- cyclen nanoparticles was added into ion solution at each titration step and then mixed for 20 minutes All measurements were performed in 0.5 M KCl pH 6.00.

## 2.4. Methods

Fourier Transform Infrared Spectroscopy (FT-IR) spectra were obtained were recorded on a Perkin Elmer Spectrum™ 3 FT-IR spectrometer with the KBr pellet technique.

Maldi-Tof mass spectra was performed on autoflex maX Brucker using α-cyano-4-hydroxycinnamic acid (CCA) as a matrix.

$^{1}$H NMR spectra were recorded in $CDCl_3$ on a Bruker Advance III 500 MHz, where tetramethylsilane (TMS) was used as the internal standard. The chemical shifts are reported in ppm, while the signal patterns are given as follows: triplet (t), doublet of triplets (dt), quartet (q) and multiplet (m).

The scanning electron microscopy (SEM) images were captured with an FEI Quanta 250 FEG (ThermoFisher Scientific) microscope, equipped with a Schottky field emission gun. The microscope was operating at 20 kV accelerating voltage in high vacuum mode.

High-resolution X-ray Photoelectron Spectroscopy (XPS) analysis was carried out using Escalab 250Xi multispectroscope (ThermoFisher Scientific). The spectroscope is equipped with an AlKα x-ray source; the pass energy through the hemispherical analyser was 20 eV. The measurement was assisted with low-energy electron and low-energy $Ar^+$ ion bombardment for charge compensation. The measurements were carried out in C 1s, Fe 2p, Si 2p and N 1s core-level binding energy range, where the adventitious C 1s spectra (284.6 eV) was used for final peak calibration. Peak deconvolution was performed using Avantage v5.9921 (ThermoFisher Scientific).

The crystalline phases and crystallite size were determined by room-temperature powder x-ray diffraction (pXRD). The pXRD patterns were collected on D2 Phaser (Brucker) diffractometer, using CuKα radiation ($\lambda$ = 1.54056 Å) with a scanning angle $2\Theta$ = 5–90° and a step size 0.01°. LeBail refinement of the pXRD pattern was performed to determine the lattice parameters, using the DIFFRAC.SUITE TOPAS.

All differential pulse anodic stripping voltammetry (DPASV) measurements were performed using an Autolab potentiostat/galvanostat (PGSTAT-128N, Methrom), equipped with NOVA 2.1.4 software. Three electrode Teflon electrochemical cell was used in all experiments to avoid metal ions sorption on the glass surface. A Static Drop Mercury Electrode (SDME) 663 VA Stand Metrohm was used as a working electrode. The reference electrode was calomel electrode $Hg|Hg_2Cl_2|KCl_{(saturated)}$ and platinum wire (Pt) were used as the counter electrode.

The detection of $Cd^{2+}$, $Pb^{2+}$, and $Cd^{2+}$ by DPASV method was performed using the following conditions: deposition time 90 s, deposition potential –0.9 V, modulation amplitude 0.05 V, modulation time 0.07 s, interval time 1.85 s, and step potential 0.003 V. The simultaneous $Cd^{2+}$, $Pb^{2+}$, and $Cd^{2+}$ ions was performed in a potential range of –0.8 V to –0.04 V, while the individual detection of ions was performed in potential range of –0,8 V to –0.5 V, – 0,6 V to –0.3 V and –0,4 V to –0.04 V for $Cd^{2+}$, $Pb^{2+}$, $Cu^{2+}$ detection, respectively.

The metal ions solutions were prepared in the supporting electrolyte, which was potassium chloride KCl 0.5 M, pH 6.0. The $Fe_3O_4$@$SiO_2$-cyclen nanoparticles suspension in supporting electrolyte solution before each measurement was freshly prepared by using ultrasonic bath for 30 minutes.

## 3. Results and discussion

### 3.1. XPS and SEM analysis

The high-resolution XPS analysis was performed to evaluate the efficiency of consecutive $Fe_3O_4$ nanoparticles functionalisation steps. The XPS spectra of each studied sample are presented in Fig. 2.

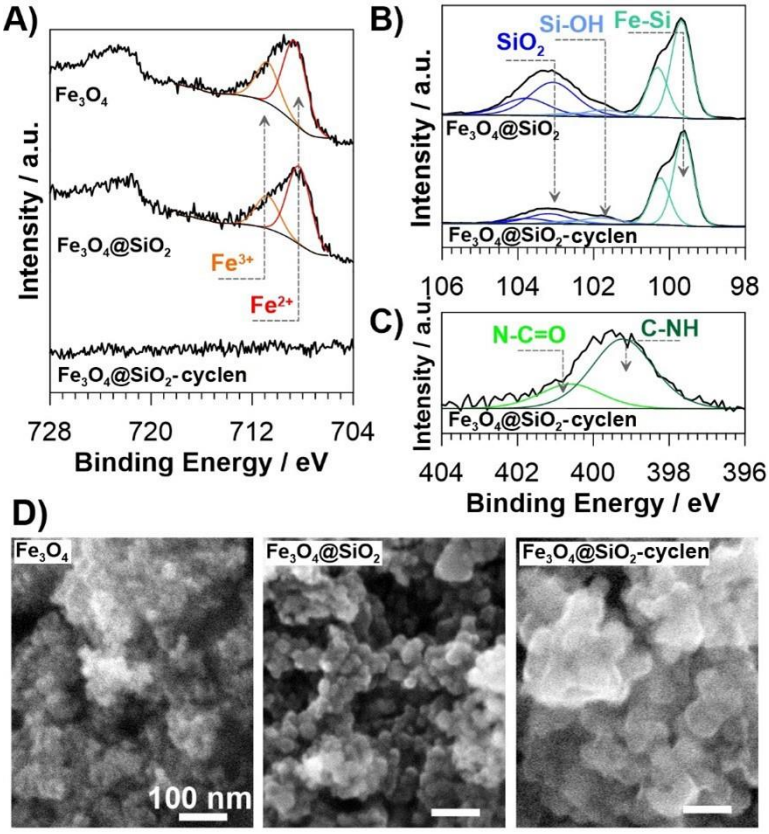

**Figure 2.** High-resolution XPS analysis of the studied $Fe_3O_4$, $Fe_3O_4@SiO_2$ and $Fe_3O_4@SiO_2$- cyclen samples in the binding energy range of: A) Fe 2p, B) Si 2p and C) N 1s peak with spectral deconvolution. D) SEM micrographs of studied materials. The scale bar marks 100 nm.

Figure 2A shows iron chemistry. The spectra obtained for the $Fe_3O_4$ sample may be deconvoluted into two Fe $2p_{3/2}$ features, peaking at 708.6 and 710.8 eV, which is characteristic of $Fe^{2+}$ and $Fe^{3+}$ in $Fe_3O_4$, respectively [54]. The calculated $Fe^{2+}$:$Fe^{3+}$ ratio is 2:1. Importantly, upon the formation of $Fe_3O_4@SiO_2$ core-shell structure, the peak position as well as the $Fe^{2+}$:$Fe^{3+}$ ratio remains unchanged, testifying to unchanged iron chemistry and structure within the nanoparticles. Nevertheless, the Fe 2p spectra intensity weakens upon the NP coverage with an $SiO_2$ shell, and eventually becomes indistinguishable for $Fe_3O_4@SiO_2$-cyclen, due to the limited depth of the XPS signal origin (approx. 3-5 nm).

The Si 2p spectra shows more complex character, with not less than three deconvolution peak doublets to be distinguished in Figure 2B. The characteristic component at 103.2 eV is attributed to $SiO_2$ while the second, smaller component negatively shifted at 0.9 eV may correspond to Si-OH bonds [55]. The third, notable component with Si $2p_{3/2}$ at 99.8 eV may have multiple origins, including Si-Fe bonds [56] or even Si-C bonds [57]. Adventitious carbon contribution in $Fe_3O_4@SiO_2$ NP powder is a relevant source for Si-C. After further modification with N-(3-(triethoxysilyl)propyl)-1,4,7,10-tetraazacyclododecane-1-carboxamide the share of 99.8 eV feature rises by 35%. This modification is assisted with two time decreases of the $SiO_2$ share, again due to the restricted depth of the XPS analysis. The detailed information are presented in **Table 1**.

**Table 1.** The chemical composition (in at.%) using XPS analysis by peak deconvolution.

| Sample | Fe 2p | | Si 2p | | | N 1s | |
|---|---|---|---|---|---|---|---|
| | $Fe^{2+}$ | $Fe^{3+}$ | $SiO_2$ | Si-OH | Si-(Fe/C) | NH-C | NC=O |
| BE / eV | 708.6 | 710.8 | 103.2 | 102.3 | 99.8 | 399.3 | 400.6 |
| $Fe_3O_4$ | 67.1 | 32.9 | -- | -- | -- | -- | -- |
| $Fe_3O_4@SiO_2$ | 1.3 | 0.6 | 40.2 | 6.9 | 50.0 | -- | -- |
| $Fe_3O_4@SiO_2$-cyclen | -- | -- | 16.4 | 9.7 | 67.4 | 4.8 | 1.7 |

While the N-(3-(triethoxysilyl)propyl)-1,4,7,10-tetraazacyclododecane-1-carboxamide compounds do not introduce C 1s features that can be easily differentiated from the surface-adsorbed adventitious carbon under air exposure, the successful $Fe_3O_4$@$SiO_2$-cyclen synthesis may be confirmed tracking N 1s spectral shape. As seen in Figure 2C this peak was deconvoluted using two separate components. The first, and more notable, at 399.3 eV is characteristic of NH-C bonds [58], while the latter, at 400.6 eV, was assigned to NC=O [59].

The morphology of each studied nanomaterial was revealed by SEM micrographs as seen in Figure 2D. The size of the $Fe_3O_4$ nanoparticles is below 20 nm, thus making it impossible for accurate estimation. Such small particle size is reported as sufficient to achieve superparamagnetism in $Fe_3O_4$ NPs [60]. Further encapsulation in $SiO_2$ by TEOS allows for full NP contours to be recognised and increasing the average size to approx. 34 ± 5 nm. This result suggests the $SiO_2$ thickness to exceed 5 nm, testifying for nearly the entire removal of the high resolution Fe 2p signal. The final functionalisation notably enlarges the $Fe_3O_4$@$SiO_2$-cyclen dimensions, which now reach 50 to as much as 100 nm. The less regular size introduced by Sil- Prop- cyclen is the probable explanation behind a significant share of Si still to be recognised by XPS.

### 3.2. pXRD analysis

The pXRD analysis was used to investigate the crystallinity nature, and size of crystallites of bare $Fe_3O_4$ nanoparticles and after each functionalisation steps. The XRD patterns of a) bare $Fe_3O_4$, b) silica-coated $Fe_3O_4$@$SiO_2$,and c) functionalised $Fe_3O_4$@$SiO_2$-cyclen nanoparticles together with the LeBail refinement (solid red line) are presented in Figure 3. A difference plot (between experimental and fitted data) and the Bragg positions are also shown in Figure 3.

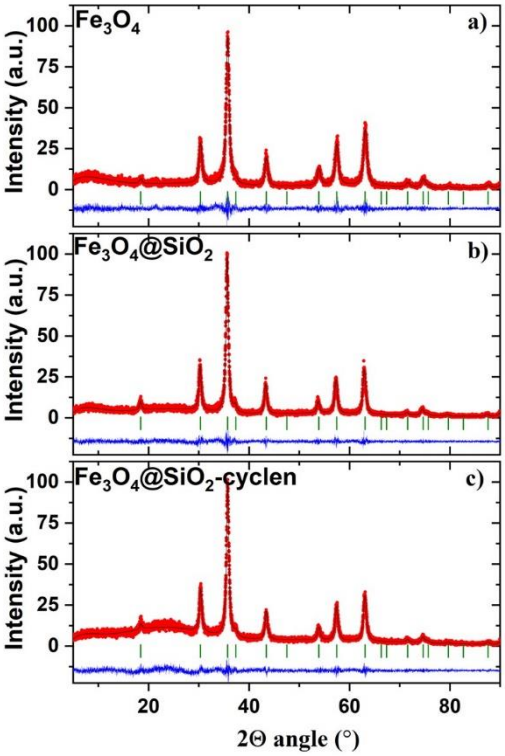


**Figure 3.** Powder x-ray diffraction pattern (pXRD) (red points) together with the LeBail refinement profile (solid black line) for a) bare $Fe_3O_4$, b) silica coated $Fe_3O_4$@$SiO_2$ and c) functionalized $Fe_3O_4$@$SiO_2$-cyclen. The green vertical bars indicate the expected Bragg peak positions for $Fe_3O_4$ (JCPDS card PDF 00-065-0731).

Our pXRD analysis confirms that for each studied sample all the diffraction peaks correspond to the cubic crystal structure (space group *Fd-3m*, no. 227). Estimated lattice parameters for the $Fe_3O_4$ phase do not differ much and are $a$ = 8.329(1) Å for bare $Fe_3O_4$, $a$ = 8.3521(6) Å for $Fe_3O_4$@$SiO_2$, and $a$ = 8.3462(6) Å for $Fe_3O_4$@$SiO_2$-cyclen nanoparticles. The average crystallite size of the $Fe_3O_4$ phase was estimated from the Scherrer formula based on the line broadening at half the maximum intensity of the reflection (220). The estimated crystallite sizes are 14, 19 and 18 nm for $Fe_3O_4$, $Fe_3O_4$@$SiO_2$, and $Fe_3O_4$@$SiO_2$-cyclen samples, respectively. The obtained results are in agreement with SEM micrographs.

### 3.3. FT-IR spectroscopy analysis

FT-IR analysis was performed to identify the appropriate functional groups present in the $Fe_3O_4$ nanoparticles at each functionalisation steps.

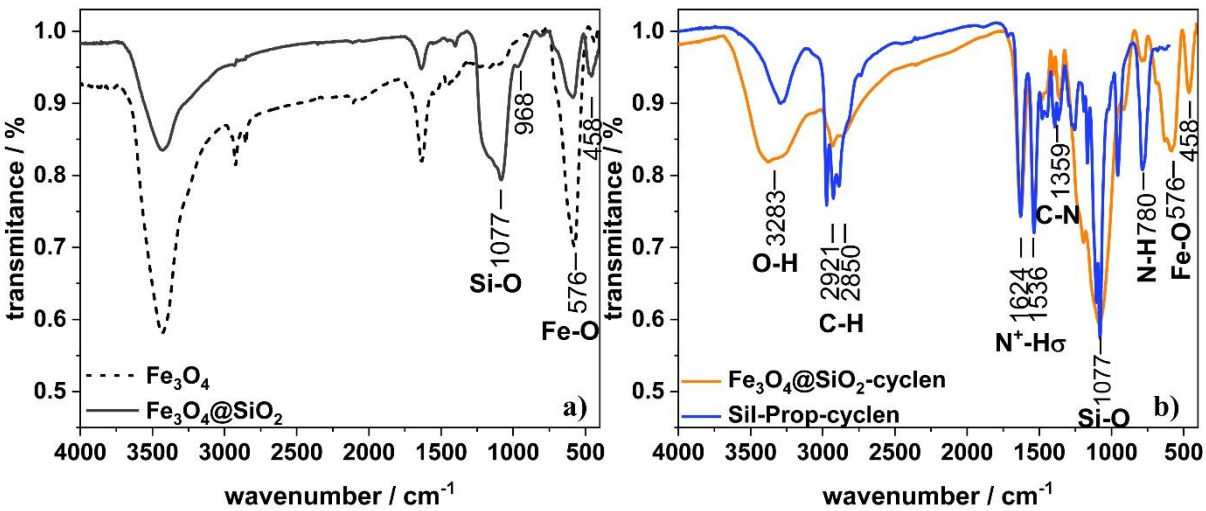


**Figure 4.** FT-IR spectra for a) bare $Fe_3O_4$, silica coated $Fe_3O_4$@$SiO_2$ and b) functionalised $Fe_3O_4$@$SiO_2$-cyclen nanoparticles, modifier silane N-(3-(triethoxysilyl)propyl)-1,4,7,10-tetraazacyclododecane-1-carboxamide (Sil-Prop-cyclen).

The $Fe_3O_4$ spectrum (Figure 4 a) shows strong stretching vibration Fe–O band at 576 $cm^{-1}$ typical for iron oxide [61]. Also observed was the reduction in the Fe–O band intensity for coated nanoparticles with silica and functional group. The band intensity decrease confirms the success in the surface functionalisation process [50]. After silica coating of nanomagnetite the intense Si–O band appeared at 1077 $cm^{-1}$. It is associated with stretching vibrations of Si–O–Si and O–Si–O on the surface of the magnetic core at 968 $cm^{-1}$ and 1077 $cm^{-1}$, respectively [62,63]. The broad strong band at 3433 $cm^{-1}$ is related to the overlapping of O–H stretching bond, which proves hydroxyl groups formation on the magnetite surface [64]. Figure 4 b blue line shows spectra for nanoparticles modifier N-(3-(triethoxysilyl)propyl)-1,4,7,10-tetraazacyclododecane-1-carboxamide for comparison. A 780 $cm^{-1}$ weak band and a two headed band about 1536 $cm^{-1}$ and 1624 $cm^{-1}$ characteristic for N–H vibrations are observed. Furthermore, there are bands that appeared at 1359 $cm^{-1}$ and about 2900 $cm^{-1}$ corresponding to C–N and N–H stretching vibrations, respectively. The same characteristic bands for the spectrum for the functionalised nanoparticles $Fe_3O_4$@$SiO_2$-cyclen (Figure 4 b orange line) are observed, which proves the success of the nanomaterials synthesis process. In addition, there is a bandwidth extension at 3283 $cm^{-1}$ which probably corresponds to overlapping O–H and N–H bands. On the basis of SEM, XPS and FT-IR analysis it can be concluded that the functionalised core-shell nanoparticles formation was conducted successfully.

### 3.3. Electrochemical analysis

In this work, the independent and simultaneous determination of $Cd^{2+}$, $Pb^{2+}$ and $Cu^{2+}$ ions was performed under optimised experimental conditions using the DPASV method and HDM electrode. 1,4,7,10-tetraazacyclododecane functionalised magnetite nanoparticles $Fe_3O_4$@$SiO_2$-cyclen were investigated as a new heavy metal ions adsorbent. To examine the ions-binding abilities of $Fe_3O_4$@$SiO_2$-cyclen, a series of measurements were performed in the solutions containing $Cd^{2+}$, $Pb^{2+}$ and $Cu^{2+}$ ions in concentration level $4.5 \cdot 10^{-6}$ M. All electrochemical experiments were performed in 0.5 M KCl pH 6.00. The pH was adjusted to avoid the formation of other metal ion species, mainly hydroxides, in the solution aside from the free ion [65–67]. The selection of pH and an influence od electrolyte was previously described by the authors in review paper [68]. There was three well-defined peaks observed at anodic stripping voltammograms at –0.65 V, –0.44 V and –0.20 V confirming the presence of $Cd^{2+}$, $Pb^{2+}$ and $Cu^{2+}$ ion, respectively. Current intensities were multiplied by the dilution factor expressed by the equation (1):

$$DF = \frac{V_0 + V_s}{V_0} \quad (1)$$

where $V_0$ is initial volume and $V_s$ is the volume of added nanoparticles suspension in a particular portion.

#### 3.3.1. $Cd^{2+}$, $Pb^{2+}$, $Cu^{2+}$ ions binding by $Fe_3O_4$@$SiO_2$-cyclen - kinetics examination

First, kinetic studies were performed to determine the effectual time to establish the equilibrium in the solution after adding the nanoparticles portion. All voltammograms were recorded immediately after adding 1 mg of $Fe_3O_4$@$SiO_2$-cyclen nanoparticles to the ion solution and after every 5 minutes of having mixed the solution. In the graph is shown the actual time that the nanoparticles stayed in the solution due to the length of the DPASV measurement (Figure 5).

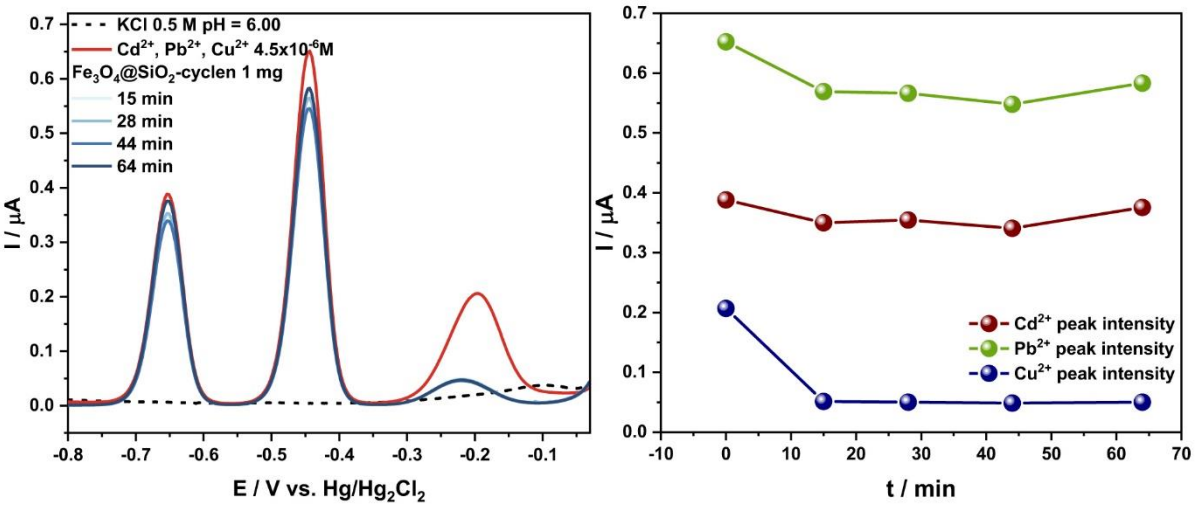


**Figure 5.** Simultaneous differential pulse anodic stripping voltammograms for examination of kinetics $Cd^{2+}$, $Pb^{2+}$ and $Cu^{2+}$ ($4.5 \cdot 10^{-6}$M) ions binding – changes of peak intensities over time after addition of 1 mg $Fe_3O_4$@$SiO_2$-cyclen nanoparticles.

After adding one portion of nanoparticles to the ion solution, a decrease in the peak intensity in the case of only the $Cu^{2+}$ ion was observed. It can be stated that the addition 1 mg of nanoparticles does not affect $Cd^{2+}$and $Pb^{2+}$ ions binding. It can be assumed that the slight peaks intensity changes are within the limit of the measurement error. On the basis of the experiment it can be concluded that the equilibrium in the solution is established no more than 15 minutes after adding the portion of nanoparticles. A different phenomenon is observed in the case of an experiment in independent $Cd^{2+}$, $Pb^{2+}$ and $Cu^{2+}$ ion solutions (Figure S1. in the Supporting Information file). In such a case, one observes a decrease in the peaks intensity over time for both the $Cd^{2+}$ and $Cu^{2+}$ ion after adding 0.5 mg $Fe_3O_4$@$SiO_2$- cyclen nanoparticles. Functionalised nanomagnetite show no tendency to $Pb^{2+}$ ions binding and it is certainly not influenced by the time of their presence in the solution. It can be assumed that in the case of $Cd^{2+}$ and $Cu^{2+}$ ions the equilibrium in the solution is established after about 50 minutes after adding the nanoparticles. After analysing the kinetics of ion binding by $Fe_3O_4$@$SiO_2$- cyclen nanoparticles, both in individual ion solutions and simultaneous analysis, it was found that the optimal time for adding the nanoparticles portion to the solution to the measurement is 20 minutes after mixing. Also, the conducted kinetics experiment suggests that the ion binding level may be influenced by the amount of added nanoparticles. Consequently, the observed

dependencies lead to the study of the $Fe_3O_4@SiO_2$- cyclen nanoparticles binding capacity by titration of the $Cd^{2+}$, $Pb^{2+}$ and $Cu^{2+}$ ions solution.

### 3.3.2. Determination of $Fe_3O_4@SiO_2$-cyclen binding ability in $Cd^{2+}$, $Pb^{2+}$ and $Cu^{2+}$ ions solutions

In order to determine the ion $Cd^{2+}$, $Pb^{2+}$ and $Cu^{2+}$ binding capacity of $Fe_3O_4@SiO_2$- cyclen nanoparticles, both in individual solutions and in the mixture, titration with nanoparticles was performed. Used as the measurement analytical method was a two-stage DPASV analysis involving pre-concentration and metal ions stripping. In the first stage, the negative potential of –0.9 V was applied to $Cd^{2+}$, $Pb^{2+}$ and $Cu^{2+}$ ions electrodeposition on the working electrode. Subsequently, the faradic current obtained by oxidation was recorded during the potential sweep toward the positive potential direction from –0,8 V to –0.5 V, from –0,6 V to –0.3 V, from –0,4 V to –0.04 V and from −0.8 V to 0.0 V, for $Cd^{2+}$, $Pb^{2+}$, $Cu^{2+}$ and simultaneous ions detection, respectively. A 0.25 mg portion of $Fe_3O_4@SiO_2$- cyclen nanoparticles was added into ion solution at each titration step and mixed for 20 minutes before starting the DPASV measurement. The mixing time was determined by the equilibrium establishment experiment in time. Peaks intensity changes during the addition of further nanoparticles portions were recalculated into sorption efficiency $R_{\%}$ (%) at every measuring step based on the formula (2) [69]:

$$R_{\%} = \frac{(C_0 - C_f)}{C_0} \cdot 100\% \quad (2)$$

where $C_0$ (mg/L) is initial ion $Me^{2+}$ concentration in the solution, $C_f$ ($C_e$) (mg/L) is the final ion concentration remaining in the solution [69].

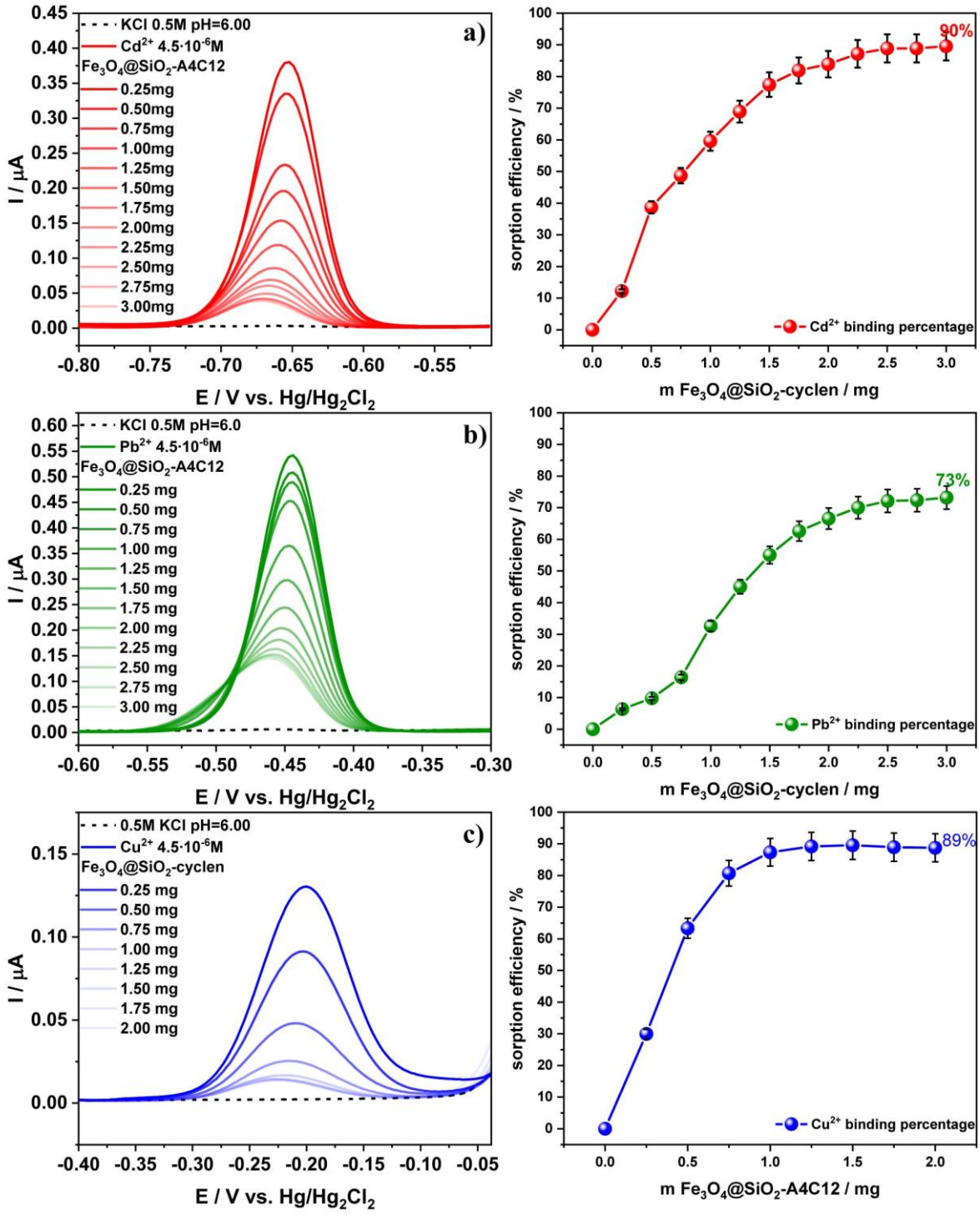


**Figure 6.** Individual differential pulse anodic stripping voltammograms and calculated sorption efficiency for a) $Cd^{2+}$, b) $Pb^{2+}$ and c) $Cu^{2+}$ ions binding by $Fe_3O_4$@$SiO_2$-cyclen nanoparticles.

Figure 6 shows an individual $Cd^{2+}$, $Pb^{2+}$ and $Cu^{2+}$ ions titration using $Fe_3O_4$@$SiO_2$- cyclen nanoparticles in portion of 0.25 mg added in every titration step. Figure 6 a) shows $Cd^{2+}$ ions binding capacity. While adding successive nanoparticles portions,

the peak intensity decreases, thus the sorption efficiency increases. After adding about 2–2.5 mg of nanoparticles, the equilibrium is established and the next portions do not affect the peak intensity reduction. The sorption effectiveness reaches about 90% and remains at this level despite nanoparticles excess. A very similar phenomenon was observed during the titration of the $Pb^{2+}$ ion (Figure 6b). Initially, the peak intensity decreases with each subsequent $Fe_3O_4$@$SiO_2$- cyclen portion so that after the addition of about 2–2.5 mg of nanoparticles, it reaches equilibrium. The titration ending determines the $Pb^{2+}$ ion sorption efficiency at a level of 73%. The $Fe_3O_4$@$SiO_2$- cyclen nanoparticles behaviour was very different in the $Cu^{2+}$ solution. Similar as in the case of $Cd^{2+}$ and $Pb^{2+}$ ions titrations, a decrease in peak intensity during titration was observed. However, a much smaller amount of nanoparticles was needed to establish equilibrium in the solution. An equilibrium establishing was observed after the addition of about 1 mg of nanoparticles. The addition of excess nanoparticles did not increase the sorption efficiency, and its level reached about 89%.

Afterwards, to compare, all three ions were titrated simultaneously by $Fe_3O_4$@$SiO_2$- cyclen nanoparticles starting with 0.25 mg for the first portion and 0.5 mg in the final steps (Figure 7).

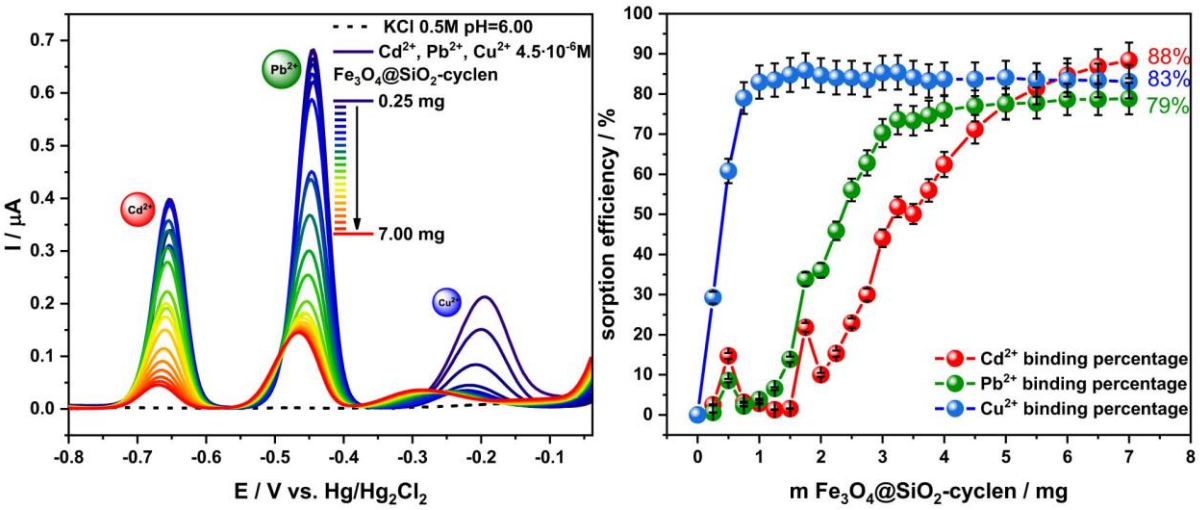


**Figure 7.** Simultaneous differential pulse anodic stripping voltammograms and calculated sorption efficiency for $Cd^{2+}$, $Pb^{2+}$, $Cu^{2+}$ ions binding by $Fe_3O_4$@$SiO_2$-cyclen nanoparticles.

In the initial titration steps, only a decrease in the intensity of the $Cu^{2+}$ peak was observed. After adding about 1–1.5 mg of nanoparticles, the percentage of $Cu^{2+}$ binding remained unchanged at a level of 83%. Then, after the $Cu^{2+}$ binding equilibrium establishing, changes in the intensity of the $Cd^{2+}$ and $Pb^{2+}$ peaks were observed. As more $Fe_3O_4$@$SiO_2$- cyclen portions are added, the intensity of the $Cd^{2+}$ and $Pb^{2+}$ peaks was reduced

and the binding efficiency increased. The $Pb^{2+}$ binding equilibrium was established after adding about 3–3.5 mg of nanoparticles to the ions solution and the sorption efficiency reached 79%. As the last equilibrium was $Cd^{2+}$ binding established after the addition stage of ion binding remains at a comparable level, however, it requires different amount of nanoparticles.

The exact calculated sorption efficiency parameters for individual (from Figure 6) and simultaneous (from Figure 7) is presented in Table 2. The sorption efficiency $R_{\%}$ calculated on the basis of the conducted DPASV experiments show that for $Cd^{2+}$ this ion was detected at similar levels of 89-88% regardless as an individual ion in solution or in a mixture of studied ions. In the case of $Pb^{2+}$, the sorption level was higher for the simultaneous solution, while for $Cu^{2+}$ sorption value was higher in the single-component. Nevertheless, the sorption efficiency are at very high levels for all analysed solutions, which confirms high efficiency of ions binding by $Fe_3O_4$@$SiO_2$-cyclen nanoparticles.

**Table 2.** Sorption efficiency parameters for individual and simultaneous $Cd^{2+}$, $Pb^{2+}$and $Cu^{2+}$ ions binding by $Fe_3O_4$@$SiO_2$- cyclen nanoparticles.

| | Individual | Simultaneous |
|---|---|---|
| | $R_{\%}$ | $R_{\%}$ |
| $Cd^{2+}$ | 89.55% | 88.37% |
| $Pb^{2+}$ | 73.20% | 78.85% |
| $Cu^{2+}$ | 88.75% | 83.08% |

### 3.3.3. Magnetic separation of adsorbed $Cd^{2+}$, $Pb^{2+}$ and $Cu^{2+}$

Finally, the separation effectiveness of nanoparticles with adsorbed heavy metal ions by external magnetic field was investigated. First, the necessary amount of nanoparticles to bind $Cd^{2+}$, $Pb^{2+}$, $Cu^{2+}$ ions solution was added to them. After that, the reduction in the metal ions peaks intensity at the DPAS voltammograms was observed (from blue line to yellow line). Then the nanoparticles contained in the solution were isolated with the use of a magnet and the solution was separated and subjected to DPASV measurement. The obtained voltammogram, apart from slightly negatively shifted potentials, shows no deviation from that obtained directly after the adsorption process. This phenomenon indicates the separation of all bound ions along with the nanoparticles from the solution (Figure 8).

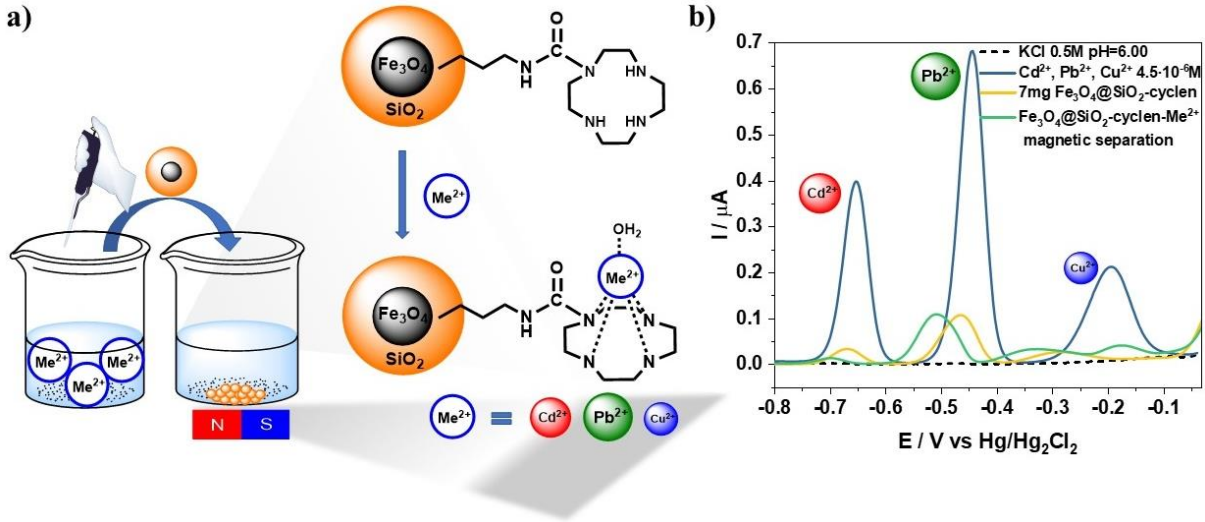


**Figure 8.** a) Scheme of magnetic $Me^{2+}$ ions binding and magnetic separation experiment. Ion binding model by aza-crown based on Subat et al. [46]. b) Simultaneous differential pulse anodic stripping voltammograms: of $Cd^{2+}$, $Pb^{2+}$, $Cu^{2+}$ ions (blue line), after adsorption by 7 mg $Fe_3O_4$@$SiO_2$-cyclen nanoparticles (yellow line) and after magnetic isolation nanoparticles with adsorbed ions (green line).

## 4. Conclusions

In this work, new core-shell nanostructures were synthesised containing a magnetic $Fe_3O_4$ core and silane shell functionalised with 1,4,7,10-tetraazacyclododecane were synthesised and characterised and their binding capacity was investigated. The results of nanomaterial characteristics using SEM, XPS, pXRD and FT-IR confirmed the success of the three-stage synthesis process.

Moreover, $Fe_3O_4$@$SiO_2$- cyclen nanoparticles binding kinetics and the sorption efficiency of $Cd^{2+}$, $Pb^{2+}$ and $Cu^{2+}$ was investigated both in individual ions solutions and in an ions mixture. Electrochemical studies proved that nanoparticles can be effectively used as adsorbents in environment heavy metal ions pollution management, which can be easily collected using an external magnetic field.

The research showed that nanoparticles have a binding tendency to all selected ions $Cd^{2+}$, $Pb^{2+}$ and $Cu^{2+}$ in their individual solutions and their sorption efficiency remains at 90%, 73% and 89%, respectively. It is worth mentioning that the smallest amount of nanoparticles was needed to bind the $Cu^{2+}$. Simultaneous $Cd^{2+}$, $Pb^{2+}$ and $Cu^{2+}$ determination also indicates the ability of $Fe_3O_4$@$SiO_2$-cyclen to bind of all ions. However, a clear order of ion binding was

observed in the mixture during the addition of further nanoparticles portions. First, $Cu^{2+}$ ions were bound, then $Pb^{2+}$ and $Cd^{2+}$ the sorption efficiency remains at 83%, 79% and 88% level, respectively. This phenomenon can be explained by the complexation constants value of these ions by 1,4,7,10-tetraazacyclododecane. The fastest $Cu^{2+}$ binding can be explained by the highest value of the complexation constant 23.9, 24.8 according to Antunes et al. [70], whereas the complexation constants of $Pb^{2+}$ and $Cd^{2+}$ are 15.9 and 14.3, respectively [70]. Additionally, the level of ion binding depends on the amount of added nanoparticles. On this basis, it can be concluded that the presence of cyclen functional groups on the surface of nanoparticles gives them the ability to bind ions. Furthermore, the $Cd^{2+}$, $Pb^{2+}$, $Cu^{2+}$ ions adsorption and magnetic separation experiment confirms the effectiveness of ion binding and purification of water environments. On the basis of this work, it can be assumed that the new nanomaterials based on $Fe_3O_4$ and functionalised with N-(3-(triethoxysilyl)propyl)-1,4,7,10-tetraazacyclododecane-1-carboxamide can be successfully used as a universal $Cd^{2+}$, $Pb^{2+}$, $Cu^{2+}$ ions magnetic adsorbent.

**Acknowledgements**

This work was created thanks to the University of Gdansk within the project supporting young scientists and PhD students (grant No. BMN 539-T050-B019-22).

**CRediT authorship contribution statement**

**Amanda Kulpa-Koterwa:** Methodology, Formal analysis, Investigation, Data Curation, Writing - Original Draft, Writing - Review & Editing, Visualization, Funding acquisition **Jacek Ryl:** Investigation, Data Curation, Writing - Original Draft, **Karolina Górnicka:** Investigation, Data Curation, Writing - Original Draft **Paweł Niedziałkowski:** Conceptualization, Resources, Writing - Original Draft, Writing - Review & Editing, Supervision

**Declaration of competing interest**

The authors declare that they have no known competing financial interests or personal relationships that could have appeared to influence the work reported in this paper.

## References


[1] S.S. Kolluru, S. Agarwal, S. Sireesha, I. Sreedhar, S.R. Kale, Heavy metal removal from wastewater using nanomaterials-process and engineering aspects, Process Safety and Environmental Protection. 150 (2021) 323–355. https://doi.org/10.1016/j.psep.2021.04.025.

[2] T.K. Das, A. Poater, Review on the Use of Heavy Metal Deposits from Water Treatment Waste towards Catalytic Chemical Syntheses, Int J Mol Sci. 22 (2021) 13383. https://doi.org/10.3390/ijms222413383.

[3] J. Briffa, E. Sinagra, R. Blundell, Heavy metal pollution in the environment and their toxicological effects on humans, Heliyon. 6 (2020) e04691. https://doi.org/10.1016/j.heliyon.2020.e04691.

[4] R.K. Gautam, S.K. Sharma, S. Mahiya, M.C. Chattopadhyaya, CHAPTER 1 Contamination of Heavy Metals in Aquatic Media: Transport, Toxicity and Technologies for Remediation, (2014) 1–24. https://doi.org/10.1039/9781782620174-00001.

[5] R. Shrestha, S. Ban, S. Devkota, S. Sharma, R. Joshi, A.P. Tiwari, H.Y. Kim, M.K. Joshi, Technological trends in heavy metals removal from industrial wastewater: A review, Journal of Environmental Chemical Engineering. 9 (2021) 105688. https://doi.org/10.1016/j.jece.2021.105688.

[6] D.-Q. Cao, X. Song, X.-M. Fang, W.-Y. Yang, X.-D. Hao, E. Iritani, N. Katagiri, Membrane filtration-based recovery of extracellular polymer substances from excess sludge and analysis of their heavy metal ion adsorption properties, Chemical Engineering Journal. 354 (2018) 866–874. https://doi.org/10.1016/j.cej.2018.08.121.

[7] A. Saeedi-Jurkuyeh, A.J. Jafari, R.R. Kalantary, A. Esrafili, A novel synthetic thin-film nanocomposite forward osmosis membrane modified by graphene oxide and polyethylene glycol for heavy metals removal from aqueous solutions, Reactive and Functional Polymers. 146 (2020) 104397. https://doi.org/10.1016/j.reactfunctpolym.2019.104397.

[8] Y. Ibrahim, E. Abdulkarem, V. Naddeo, F. Banat, S.W. Hasan, Synthesis of super hydrophilic cellulose-alpha zirconium phosphate ion exchange membrane via surface coating for the removal of heavy metals from wastewater, Science of The Total Environment. 690 (2019) 167–180. https://doi.org/10.1016/j.scitotenv.2019.07.009.

[9] S. Platzer, M. Kar, R. Leyma, S. Chib, A. Roller, F. Jirsa, R. Krachler, D.R. MacFarlane, W. Kandioller, B.K. Keppler, Task-specific thioglycolate ionic liquids for heavy metal extraction: Synthesis, extraction efficacies and recycling properties, Journal of Hazardous Materials. 324 (2017) 241–249. https://doi.org/10.1016/j.jhazmat.2016.10.054.

[10] Y. Deng, C. Feng, L. Tang, G. Zeng, Z. Chen, M. Zhang, Chapter 5 - Nanohybrid Photocatalysts for Heavy Metal Pollutant Control, in: L. Tang, Y. Deng, J. Wang, J. Wang, G. Zeng (Eds.), Nanohybrid and Nanoporous Materials for Aquatic Pollution Control, Elsevier, 2019: pp. 125–153. https://doi.org/10.1016/B978-0-12-814154-0.00005-0.

[11] X. Guan, X. Yuan, Y. Zhao, H. Wang, H. Wang, J. Bai, Y. Li, Application of functionalized layered double hydroxides for heavy metal removal: A review, Science of The Total Environment. (2022) 155693. https://doi.org/10.1016/j.scitotenv.2022.155693.

[12] C. Yan, Z. Qu, J. Wang, L. Cao, Q. Han, Microalgal bioremediation of heavy metal pollution in water: Recent advances, challenges, and prospects, Chemosphere. 286 (2022) 131870. https://doi.org/10.1016/j.chemosphere.2021.131870.

[13] J. He, J.P. Chen, A comprehensive review on biosorption of heavy metals by algal biomass: Materials, performances, chemistry, and modeling simulation tools,

Bioresource Technology. 160 (2014) 67–78. https://doi.org/10.1016/j.biortech.2014.01.068.
[14] L. Yang, J. Wang, Y. Yang, S. Li, T. Wang, P. Oleksak, Z. Chrienova, Q. Wu, E. Nepovimova, X. Zhang, K. Kuca, Phytoremediation of heavy metal pollution: Hotspots and future prospects, Ecotoxicology and Environmental Safety. 234 (2022) 113403. https://doi.org/10.1016/j.ecoenv.2022.113403.
[15] Q. Chen, Y. Yao, X. Li, J. Lu, J. Zhou, Z. Huang, Comparison of heavy metal removals from aqueous solutions by chemical precipitation and characteristics of precipitates, Journal of Water Process Engineering. 26 (2018) 289–300. https://doi.org/10.1016/j.jwpe.2018.11.003.
[16] A.J. Bora, R.K. Dutta, Removal of metals (Pb, Cd, Cu, Cr, Ni, and Co) from drinking water by oxidation-coagulation-absorption at optimized pH, Journal of Water Process Engineering. 31 (2019) 100839. https://doi.org/10.1016/j.jwpe.2019.100839.
[17] A. Jain, S. Rai, R. Srinivas, R.I. Al-Raoush, Bioinspired modeling and biogeography-based optimization of electrocoagulation parameters for enhanced heavy metal removal, Journal of Cleaner Production. 338 (2022) 130622. https://doi.org/10.1016/j.jclepro.2022.130622.
[18] S. Shukla, R. Khan, A. Daverey, Synthesis and characterization of magnetic nanoparticles, and their applications in wastewater treatment: A review, Environmental Technology & Innovation. 24 (2021) 101924. https://doi.org/10.1016/j.eti.2021.101924.
[19] R.M. Ali, H.A. Hamad, M.M. Hussein, G.F. Malash, Potential of using green adsorbent of heavy metal removal from aqueous solutions: Adsorption kinetics, isotherm, thermodynamic, mechanism and economic analysis, Ecological Engineering. 91 (2016) 317–332. https://doi.org/10.1016/j.ecoleng.2016.03.015.
[20] D. Saritha, A concise review on the removal of heavy metals from wastewater using adsorbents, Materials Today: Proceedings. 63 (2022) 3973–3977. https://doi.org/10.1016/j.matpr.2022.04.579.
[21] U. Haripriyan, K.P. Gopinath, J. Arun, Chitosan based nano adsorbents and its types for heavy metal removal: A mini review, Materials Letters. 312 (2022) 131670. https://doi.org/10.1016/j.matlet.2022.131670.
[22] I. Ihsanullah, M. Sajid, S. Khan, M. Bilal, Aerogel-based adsorbents as emerging materials for the removal of heavy metals from water: Progress, challenges, and prospects, Separation and Purification Technology. 291 (2022) 120923. https://doi.org/10.1016/j.seppur.2022.120923.
[23] Y. Yue, Y. Liu, W. Zhang, J. Guo, Y. Gong, Y. Yu, Amidoxime functionalized low-cost cellulose-based adsorbent derived from waste cigarette filters for efficient heavy metal removal, Journal of Environmental Chemical Engineering. 10 (2022) 107846. https://doi.org/10.1016/j.jece.2022.107846.
[24] H. Zhang, X. Hu, T. Li, Y. Zhang, H. Xu, Y. Sun, X. Gu, C. Gu, J. Luo, B. Gao, MIL series of metal organic frameworks (MOFs) as novel adsorbents for heavy metals in water: A review, Journal of Hazardous Materials. 429 (2022) 128271. https://doi.org/10.1016/j.jhazmat.2022.128271.
[25] C. Duan, T. Ma, J. Wang, Y. Zhou, Removal of heavy metals from aqueous solution using carbon-based adsorbents: A review, Journal of Water Process Engineering. 37 (2020) 101339. https://doi.org/10.1016/j.jwpe.2020.101339.
[26] S. Cho, J.-H. Kim, K.S. Yang, M. Chang, Facile preparation of amino-functionalized polymeric microcapsules as efficient adsorbent for heavy metal ions removal, Chemical Engineering Journal. 425 (2021) 130645. https://doi.org/10.1016/j.cej.2021.130645.
[27] E. Vunain, A. Mishra, B. Mamba, Dendrimers, mesoporous silicas and chitosan-based nanosorbents for the removal of heavy-metal ions: A review, International Journal of

Biological Macromolecules. 86 (2016) 570–586. https://doi.org/10.1016/j.ijbiomac.2016.02.005.
[28] M.M. Al-Mahadeen, A.G. Jiries, S.A. Al-Trawneh, S.F. Alshahateet, A.S. Eldouhaibi, S. Sagadevan, Kinetics and equilibrium studies for the removal of heavy metal ions from aqueous solution using the synthesized C-4-bromophenylcalix[4]resorcinarene adsorbent, Chemical Physics Letters. 783 (2021) 139053. https://doi.org/10.1016/j.cplett.2021.139053.
[29] Z. Cheng, J. Yang, L. Li, Y. Chen, X. Wang, Flocculation inspired combination of layered double hydroxides and fulvic acid to form a novel composite adsorbent for the simultaneous adsorption of anionic dye and heavy metals, Journal of Colloid and Interface Science. 618 (2022) 386–398. https://doi.org/10.1016/j.jcis.2022.03.097.
[30] R. Torkaman, F. Maleki, M. Gholami, M. Torab-Mostaedi, M. Asadollahzadeh, Assessing the radiation-induced graft polymeric adsorbents with emphasis on heavy metals removing: A systematic literature review, Journal of Water Process Engineering. 44 (2021) 102371. https://doi.org/10.1016/j.jwpe.2021.102371.
[31] V. Vinayagam, S. Murugan, R. Kumaresan, M. Narayanan, M. Sillanpää, D.-V.N. Vo, O.S. Kushwaha, Protein nanofibrils as versatile and sustainable adsorbents for an effective removal of heavy metals from wastewater: A review, Chemosphere. 301 (2022) 134635. https://doi.org/10.1016/j.chemosphere.2022.134635.
[32] J. R., B. Gurunathan, S. K, S. Varjani, H.H. Ngo, E. Gnansounou, Advancements in heavy metals removal from effluents employing nano-adsorbents: Way towards cleaner production, Environmental Research. 203 (2022) 111815. https://doi.org/10.1016/j.envres.2021.111815.
[33] R. Bhateria, R. Singh, A review on nanotechnological application of magnetic iron oxides for heavy metal removal, Journal of Water Process Engineering. 31 (2019) 100845. https://doi.org/10.1016/j.jwpe.2019.100845.
[34] A. Latif, D. Sheng, K. Sun, Y. Si, M. Azeem, A. Abbas, M. Bilal, Remediation of heavy metals polluted environment using Fe-based nanoparticles: Mechanisms, influencing factors, and environmental implications, Environmental Pollution. 264 (2020) 114728. https://doi.org/10.1016/j.envpol.2020.114728.
[35] F. Ghorbani, S. Kamari, Core–shell magnetic nanocomposite of Fe3O4@SiO2@NH2 as an efficient and highly recyclable adsorbent of methyl red dye from aqueous environments, Environmental Technology & Innovation. 14 (2019) 100333. https://doi.org/10.1016/j.eti.2019.100333.
[36] S. Patil, R. Tandon, N. Tandon, A current research on silica coated ferrite nanoparticle and their application: Review, Current Research in Green and Sustainable Chemistry. 4 (2021) 100063. https://doi.org/10.1016/j.crgsc.2021.100063.
[37] L. Wang, X. Huang, C. Wang, X. Tian, X. Chang, Y. Ren, S. Yu, Applications of surface functionalized Fe3O4 NPs-based detection methods in food safety, Food Chemistry. 342 (2021) 128343. https://doi.org/10.1016/j.foodchem.2020.128343.
[38] S. Jin, B.C. Park, W.S. Ham, L. Pan, Y.K. Kim, Effect of the magnetic core size of amino-functionalized Fe3O4-mesoporous SiO2 core-shell nanoparticles on the removal of heavy metal ions, Colloids and Surfaces A: Physicochemical and Engineering Aspects. 531 (2017) 133–140. https://doi.org/10.1016/j.colsurfa.2017.07.086.
[39] Y. Harinath, D.H.K. Reddy, L.S. Sharma, K. Seshaiah, Development of hyperbranched polymer encapsulated magnetic adsorbent (Fe3O4@SiO2–NH2-PAA) and its application for decontamination of heavy metal ions, Journal of Environmental Chemical Engineering. 5 (2017) 4994–5001. https://doi.org/10.1016/j.jece.2017.09.031.
[40] N. Naini, H. Sid Kalal, M.R. Almasian, D. Niknafs, M. Taghiof, H. Hoveidi, Phosphine-functionalized Fe3O4/SiO2/composites as efficient magnetic nanoadsorbents for the

removal of palladium ions from aqueous solution: Kinetic, thermodynamic and isotherm studies, Materials Chemistry and Physics. 287 (2022) 126242. https://doi.org/10.1016/j.matchemphys.2022.126242.

[41] E. Ragheb, M. Shamsipur, F. Jalali, F. Mousavi, Modified magnetic-metal organic framework as a green and efficient adsorbent for removal of heavy metals, Journal of Environmental Chemical Engineering. 10 (2022) 107297. https://doi.org/10.1016/j.jece.2022.107297.

[42] W. Qin, S. Xu, G. Xu, Q. Xie, C. Wang, Z. Xu, Preparation of silica gel bound crown ether and its extraction performance towards zirconium and hafnium, Chemical Engineering Journal. 225 (2013) 528–534. https://doi.org/10.1016/j.cej.2013.03.127.

[43] M. Subat, K. Woinaroschy, S. Anthofer, B. Malterer, B. König, 1,4,7,10-Tetraazacyclododecane Metal Complexes as Potent Promoters of Carboxyester Hydrolysis under Physiological Conditions, Inorg. Chem. 46 (2007) 4336–4356. https://doi.org/10.1021/ic070101z.

[44] J.M. Park, O.J. Shon, H. Hong, J.S. Kim, Y. Kim, H.B. Lim, Development of a microchip metal ion sensor using dinitro-azocalix[4]azacrown, Microchemical Journal. 80 (2005) 139–144. https://doi.org/10.1016/j.microc.2004.07.017.

[45] B. König, M. Pelka, M. Subat, I. Dix, P.G. Jones, Urea Derivatives of 1,4,7,10-Tetraazacyclododecane − Synthesis and Binding Properties, European Journal of Organic Chemistry. 2001 (2001) 1943–1949. https://doi.org/10.1002/1099-0690(200105)2001:10<1943::AID-EJOC1943>3.0.CO;2-O.

[46] M. Subat, K. Woinaroschy, C. Gerstl, B. Sarkar, W. Kaim, B. König, 1,4,7,10-Tetraazacyclododecane Metal Complexes as Potent Promoters of Phosphodiester Hydrolysis under Physiological Conditions, Inorg. Chem. 47 (2008) 4661–4668. https://doi.org/10.1021/ic702413q.

[47] M. Regueiro-Figueroa, E. Ruscsák, L. Fra, G. Tircsó, I. Tóth, A. de Blas, T. Rodríguez-Blas, C. Platas-Iglesias, D. Esteban-Gómez, Highly Stable Complexes of Divalent Metal Ions (Mg2+, Ca2+, Cu2+, Zn2+, Cd2+, and Pb2+) with a Dota-Like Ligand Containing a Picolinate Pendant, European Journal of Inorganic Chemistry. 2014 (2014) 6165–6173. https://doi.org/10.1002/ejic.201402693.

[48] P. Antunes, P.M. Campello, R. Delgado, M.G.B. Drew, V. Félix, I. Santos, Metal complexes of a tetraazacyclophane: solution and molecular modelling studies, Dalton Trans. (2003) 1852–1860. https://doi.org/10.1039/B301033C.

[49] P. Niedziałkowski, D. Zarzeczańska, T. Ossowski, Synthesis and Characterization of 1,4,7,10-Tetraazacyclododecane Derivatives and Their Metal Complexes, Polish Journal of Chemistry. Vol. 82 (2008) 1175–1197.

[50] A. Kulpa, J. Ryl, G. Skowierzak, A. Koterwa, G. Schroeder, T. Ossowski, P. Niedziałkowski, Comparison of Cadmium Cd2+ and Lead Pb2+ Binding by Fe2O3@SiO2-EDTA Nanoparticles – Binding Stability and Kinetic Studies, Electroanalysis. 32 (2020) 588–597. https://doi.org/10.1002/elan.201900616.

[51] A. Kulpa, J. Ryl, G. Schroeder, A. Koterwa, J. Sein Anand, T. Ossowski, P. Niedziałkowski, Simultaneous voltammetric determination of Cd2+, Pb2+, and Cu2+ ions captured by Fe3O4@SiO2 core-shell nanostructures of various outer amino chain length, Journal of Molecular Liquids. 314 (2020) 113677. https://doi.org/10.1016/j.molliq.2020.113677.

[52] S. Sawan, R. Maalouf, A. Errachid, N. Jaffrezic-Renault, Metal and metal oxide nanoparticles in the voltammetric detection of heavy metals: A review, TrAC Trends in Analytical Chemistry. 131 (2020) 116014. https://doi.org/10.1016/j.trac.2020.116014.

[53] T. Matsuoka, S. Yamamoto, O. Moriya, M. Kashio, T. Sugizaki, Synthesis of thermoresponsive polysilsesquioxane with methoxyethylamide group and crown ether, Polym J. 42 (2010) 313–318. https://doi.org/10.1038/pj.2010.7.
[54] M.C. Biesinger, B.P. Payne, A.P. Grosvenor, L.W.M. Lau, A.R. Gerson, R.St.C. Smart, Resolving surface chemical states in XPS analysis of first row transition metals, oxides and hydroxides: Cr, Mn, Fe, Co and Ni, Applied Surface Science. 257 (2011) 2717–2730. https://doi.org/10.1016/j.apsusc.2010.10.051.
[55] Š. Meškinis, A. Vasiliauskas, M. Andrulevičius, D. Peckus, S. Tamulevičius, K. Viskontas, Diamond Like Carbon Films Containing Si: Structure and Nonlinear Optical Properties, Materials. 13 (2020) 1003. https://doi.org/10.3390/ma13041003.
[56] F. Sirotti, M. De Santis, G. Rossi, Synchrotron-radiation photoemission and x-ray absorption of Fe silicides, Phys. Rev. B. 48 (1993) 8299–8306. https://doi.org/10.1103/PhysRevB.48.8299.
[57] R. Bywalez, H. Karacuban, H. Nienhaus, C. Schulz, H. Wiggers, Stabilization of mid-sized silicon nanoparticles by functionalization with acrylic acid, Nanoscale Research Letters. 7 (2012) 76. https://doi.org/10.1186/1556-276X-7-76.
[58] A. Mohtasebi, T. Chowdhury, L.H.H. Hsu, M.C. Biesinger, P. Kruse, Interfacial Charge Transfer between Phenyl-Capped Aniline Tetramer Films and Iron Oxide Surfaces, J. Phys. Chem. C. 120 (2016) 29248–29263. https://doi.org/10.1021/acs.jpcc.6b09950.
[59] A. Tanver, M.-H. Huang, Y. Luo, Energetic interpenetrating polymer network (EIPN): enhanced thermo-mechanical properties of NCO-fMWCNTs/HTPB PU and alkyne-fMWCNTs/acyl-GAP based nanocomposite and its propellants, RSC Adv. 6 (2016) 49101–49112. https://doi.org/10.1039/C6RA07742K.
[60] Q. Li, C.W. Kartikowati, S. Horie, T. Ogi, T. Iwaki, K. Okuyama, Correlation between particle size/domain structure and magnetic properties of highly crystalline Fe3O4 nanoparticles, Sci Rep. 7 (2017) 9894. https://doi.org/10.1038/s41598-017-09897-5.
[61] F. Shalali, S. Cheraghi, M.A. Taher, A sensitive electrochemical sensor amplified with ionic liquid and N-CQD/Fe3O4 nanoparticles for detection of raloxifene in the presence of tamoxifen as two essentials anticancer drugs, Materials Chemistry and Physics. 278 (2022) 125658. https://doi.org/10.1016/j.matchemphys.2021.125658.
[62] T. Yousofi, A. Rahmati, Fe3O4@SiO2-BU core-shell as a new nanomagnetic gelator for oil recovery from water, Polyhedron. 180 (2020) 114363. https://doi.org/10.1016/j.poly.2020.114363.
[63] T. Akbarpour, J. Yousefi Seyf, A. Khazaei, N. Sarmasti, Synthesis of Pyrano [2,3-c] Pyrazole Derivatives Using a Novel Ionic-Liquid Based Nano-Magnetic Catalyst (Fe 3 O 4 @SiO 2 @(CH 2 ) 3 NH@CC@Imidazole@SO 3 H + Cl − ), Polycyclic Aromatic Compounds. (2021) 1–21. https://doi.org/10.1080/10406638.2021.1873152.
[64] D. Chen, T. Awut, B. Liu, Y. Ma, T. Wang, I. Nurulla, Functionalized magnetic Fe3O4 nanoparticles for removal of heavy metal ions from aqueous solutions, E-Polymers. 16 (2016) 313–322. https://doi.org/10.1515/epoly-2016-0043.
[65] Q. Kong, C. Wei, S. Preis, Y. Hu, F. Wang, Facile preparation of nitrogen and sulfur co-doped graphene-based aerogel for simultaneous removal of Cd2+ and organic dyes, Environ Sci Pollut Res Int. 25 (2018) 21164–21175. https://doi.org/10.1007/s11356-018-2195-8.
[66] T. Chen, H. Li, H. Wang, X. Zou, H. Liu, D. Chen, Y. Zhou, Removal of Pb(II) from Aqueous Solutions by Periclase/Calcite Nanocomposites, Water Air Soil Pollut. 230 (2019) 299. https://doi.org/10.1007/s11270-019-4354-z.
[67] J. Liu, D. Luo, L. Huang, Y. Wang, S. Wen, Copper adsorption reaction rate and ion exchange ratio during the copper activation of sphalerite, Physicochem. Probl. Miner. Process. 54 (2017) 377–385. https://doi.org/10.5277/ppmp1832.

[68] A. Kulpa-Koterwa, T. Ossowski, P. Niedziałkowski, Functionalized Fe3O4 Nanoparticles as Glassy Carbon Electrode Modifiers for Heavy Metal Ions Detection—A Mini Review, Materials. 14 (2021) 7725. https://doi.org/10.3390/ma14247725.
[69] C. Zeng, P. Liu, Z. Xiao, Y. Li, L. Song, Z. Cao, D. Wu, Y.-F. Zhang, Highly Selective Adsorption and Recovery of Palladium from Spent Catalyst Wastewater by 1,4,7,10-Tetraazacyclododecane-Modified Mesoporous Silica, ACS Sustainable Chem. Eng. 10 (2022) 1103–1114. https://doi.org/10.1021/acssuschemeng.1c05915.
[70] P. Antunes, P.M. Campello, R. Delgado, M.G.B. Drew, V. Félix, I. Santos, Metal complexes of a tetraazacyclophane: solution and molecular modelling studies, Dalton Trans. (2003) 1852–1860. https://doi.org/10.1039/B301033C.